The effect of closed cycle of air flow circulation on the thermal performance of solar air collector

D Bensahal and A Yousfi

Laboratory of Mechanic, Faculty of Technology, University of Laghouat, Laghouat (03000), Algeria

E-mail: bensahal.dz@gmail.com

Abstract

This experimental study aims to investigate the effect of the closed cycle of air circulation on the thermal performance of the solar air collector with attached fins in the site of Laghouat in Algeria, under climatic conditions. Our experimental procedure includes two types of cycles: open cycle and closed cycle. For each cycle, we have considered two tilt angle: 0 and 30 degree. Moreover, the solar collector is oriented in a southerly direction with a definite angle of inclination. The flow rate used in experiment is equal to 0.0129402 m^3/s. Then, by comparing the experimental and theoretical results, we observe that the maximum temperature difference between the outlet and inlet air for the open cycle (27 °C, at 14h30) is higher than that of the close cycle (17 °C, at 14h00). The maximum efficiencies obtained for the open cycle for the both configurations were η(30 degrees)=25.29% and η(0 degree)=35.71% at 4 pm. These values are higher than those of the maximum efficiencies of the closed cycle with η(30 degrees)=7.86% at 4 pm and η(0 degree)=13.31% at 12h00, respectively.

Keywords: thermal efficiency, closed cycle, air flow rate, solar air collector

Nomenclature

T	temperature (^{o}C)
L	length of solar air collector (m)
l	Width of solar air collector (m)
$\dot{m}$	Mass flow (kg/s)
V	fluid velocity (m/s)
It	solar irradiation intensity (W/m^2)
Qu	the useful energy gain (W)
Cp	specific heat of the air (j/kg.°K)
Ac	the area of the collector (m^2)

Greek symbols

α	absorptivity
β	tilt angle (solar collector - ground) (degree)
ρ	density (kg/m^3)
ε	emissivity
η	thermal efficiency
τ	transmitance

Subscripts

hc	convective transfer coefficient [W/(m^2.K)]
hr	radiative transfer coefficient [W/(m^2.K)]
hd	conductive transfer coefficient [W/(m^2.K)]
p	absorber
pl	bottom plate
v	transparent cover or glass
c, ab	sky, ambient
f, s	fluide, ground
is	insulating plate

1. Introduction

The use of energy in daily life is increasing more and more knowing that the use of fossil fuels is harmful to humanitarian life. For this, the search for a source friendly to human life and renewable is very interesting. Solar energy satisfies this need knowing that it can be exploited in many applications such as: water and house heating and the production of electrical energy or fruit drying [1-5]. Much research shows that the implantation of obstacles in the flow vein of the fluid promotes the occurrence of turbulence which leads to the increase in the rate of heat transfer. Different geometries for artificial roughness with different materials which have a higher conduction coefficient are used in order to increase or improve the thermal performance of solar collectors. The addition of the baffles improves the heat transfer coefficient by convection from the absorber to the air. Studies show that it is the most efficient way
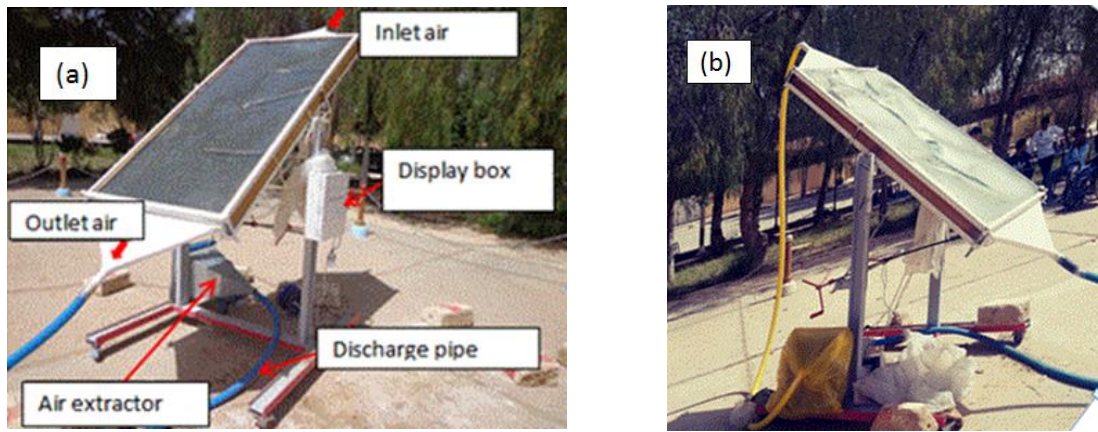
Figure 1. A photo of the experimental setup in the operating state: (a) open cycle of air and (b) closed cycle of air.

from a heat transfer point of view and on the other hand less expensive from the economic side [6-8]. Even for natural convection, adding baffles below the absorber increases heat transfer by about 20% as shown in the study of Pakdaman et al. [9] or by using porous medium as reported by Gizem [10].

The increase in thermal efficiency is achieved through the increase of the exchange or transfer surface area using baffles [11-14] which subsequently creates turbulence [15-16]. The transfer can take different ways such as using the tube heat exchanger, cross-corrugated and multi-pass flat-plate solar air heaters with external recycle [17-20].

In this study, we tried to present the effects of the closed air circuit cycle on the thermal performance of solar air collector with attached fins and single air pass in the region of Laghouat, Algeria (latitude: 33°47′59″ N, longitude: 2°51′54″ E, elevation: 764 m).

2. Methodology and experimental setup

The tests taken during the experiments include the following parameters: the global solar radiation, the air inlet and outlet temperature, the ambient temperature, the temperature of the absorber and the bottom plate and finally the air flow rate. The design and manufacture of the solar air collector was carried out in the mechanical laboratory. The solar air collector was oriented in a southerly direction and with a tilt angle of 0 degree and 30 degrees. The test day begins at 9:00 a.m. and ends at 4:00 p.m.

2. 1 Governing equations

The establishment of the energy balance takes into accounts the solar energy absorbed by the absorber plate and the useful thermal energy of the system accompanied by certain energy losses [14]. The thermal equilibrium of the transparent cover is:

$$-(T_v - T_{ab}).h_{c\_v} - (T_v - T_c).h_{rv\_c} - (T_v - T_s).h_{rv\_s}$$
$$+(T_v - T_p).\left\{ \frac{h_{c\_nat}}{2} + h_{rp\_v} \right\} + \alpha_v.I_t = 0 \qquad (1)$$

The thermal equilibrium of the absorber is:

$$-(T_P - T_v).\left\{ \frac{h_{c\_nat}}{r} + h_{rp\_v} \right\} - (T_P - T_f).h_{cp\_f}$$
$$-(T_P - T_{pl}).h_{rp\_pl} + \tau_v.\alpha_p.I_t = 0 \qquad (2)$$

The thermal equilibrium of the heat transfer fluid is:

$$(T_P - T_f).h_{cp\_f} - (T_f - T_{pl}).h_{cpl\_f} - dQu/(l.dx) = 0 \qquad (3)$$

The thermal equilibrium of the bottom plate is:

$$(T_f - T_{pl}).h_{cpl\_f} + (T_p - T_{pl}).h_{rp\_pl} - (T_{pl} - T_{is}).h_d = 0 \qquad (4)$$

The thermal equilibrium of the external insulating plate is given by the following equation:

$$(T_{pl} - T_{is}).h_d - (T_{is} - T_{ab}).h_{c\_v} - (T_{is} - T_s).h_{ris\_s} = 0 \qquad (5)$$

We obtained a system of 5 equations for 5 unknowns which represent the temperatures put in the form of a vector T_i (T_v, T_p, T_f, T_{pl} et T_{is}) which will be solved by the numerical method. For the resolution, the matrix form is: $[A_{ij}] [T_i] = [C_i]$. The theoretical results obtained by solving these equations (program) that will be object of comparison later with experimental results.

The thermal efficiency (%) of the solar air collector is defined by the following equation [2]:

$$\eta = \overset{\bullet}{m}.Cp.\frac{\left(T_{out} - T_{in} \right)}{I_t.\, A_c}, \qquad (6)$$

where, the masse flow rate is:

$$m = \rho \cdot V, \qquad (7)$$

The specific heat of air is expressed as:

$$Cp = 999.23 + 0.1434\,T_f + 1.101.10^{-4}\,T_f^2$$
$$- 6.7581.10^{-8}\,T_f^3, \qquad (8)$$

The useful energy is given by:

$$Q_u = m \cdot C_p \ (T_{out} - T_{in}), \qquad (9)$$

The density of air is given by the following equation (Eq.(10)):

$$\rho = 1.204 \left(\frac{293}{T_f} \right). \qquad (10)$$

2. 2 Experimental setup and measurement procedure

A photo of our experimental setup with a single flow between the absorber and bottom plates is presented in figure 1 with attached fins located under the absorber plate of the solar air collector. Two operating states are studied. The first is an open cycle of circulation of air which means that the inlet and the outlet of the air are not connected to each other. Here, the speed of air is ensured by the air extractor (fan). The second state is a closed cycle of circulation of air which signifies that the
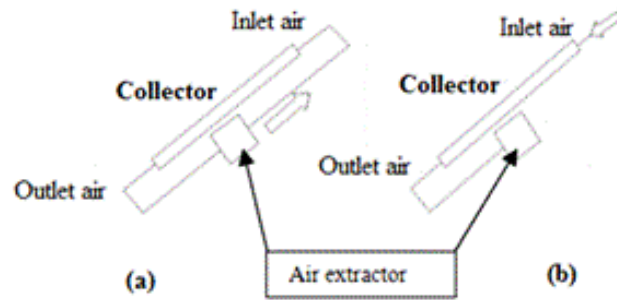
Figure 2. The experimental set up of a) closed cycle, b) open cycle.
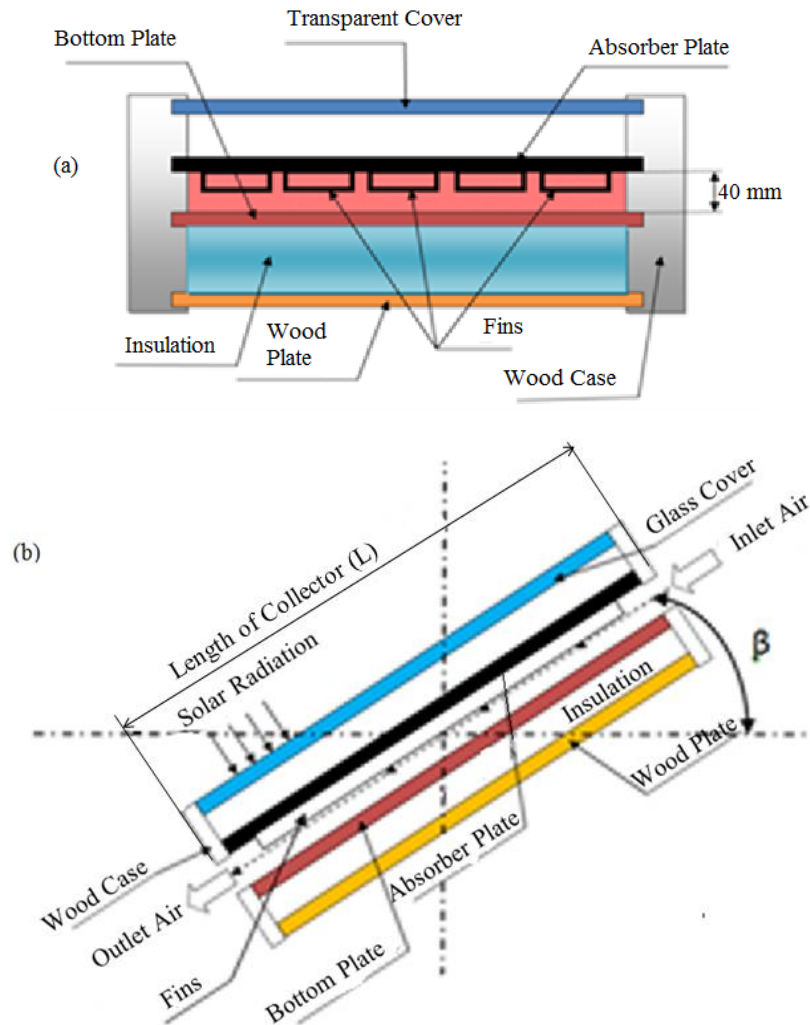

Figure 3. Solar air collector: a) cross section and b) longitudinal section.

inlet and outlet air are connected to each other as shown in figure 2 (a) and (b), respectively.

The experimental device is composed of a Plexiglas plate characterized by a transmission coefficient τ = 0.9 and a thickness of 4 mm and two galvanized steel plates with a thickness of 1 mm and physical characteristics (α = 0.95 and ε = 0.95) one for the absorber and the other for the bottom plate. The height of the mobile air stream is 40 mm. Rear insulation is provided by a 40 mm thick polystyrene sheet. The set is placed in a wooden case. Five fins with rectangular form are placed under the

absorber plate with 1.88 m length and 0.01 m thickness. The distance between two adjacent fins is 73.3 mm and the fins thickness is 1 mm, as shown in figure 3.

The height of stagnant air layer between the transparent cover and the absorber plate was 0.02 m. All the geometrical dimensions and thermo-physical characteristics are reported in tables 1 and 2. The solar air collector contains five fins as well. Each fin has dimensions of 1.88 m length, 0.1 m width, and 1 mm thickness. The height of the fin is equal to 10 mm while the distance between two fins is equivalent to 73.3 mm.

Table 1. The dimensions of the components of the solar air heater.

Component	Length (m)	Width (m)	Thickness (mm)	Number of fins	Height of fin (mm)	Distance between two fins (mm)
Transparent cover	1.94	0.94	4	-	-	-
Absorber	1.94	0.94	1	-	-	-
Bottom plate	1.94	0.94	1	-	-	-
Insulation	1.94	0.94	40	-	-	-
Wood Case	2	1	80	-	-	-

Table 2. Thermo-physical characteristics of the different constituents [2].

Component	Materials	density (kg/m³)	Specific heat (j/kg.K)	Thermal conductivity (W/m.K)
Transparent cover	Plexiglass	1.2	1500	1.5
Absorber, bottom plate and fins	Galvanized iron	7800	473	45
Insulation	Expanded polystyrene	16	1670	0.037

Table 3. The experimental conditions: angle, flow rate, time of day and condition of the sky.

No	Type of cycle flow	Angle of inclination (degree)	Flow rate (m³/s)	Date	Sky conditions
1	Open	0	0.0129402	11.02.2019	clear
2	Open	30	0.0129402	18.02.2019	clear
3	Closed	0	0.0129402	08.04.2019	partial
4	Closed	30	0.0129402	14.04.2019	clear

The temperatures are acquired manually using a set of 11 thermocouples (model: DC-M02) distributed over the absorber and the bottom plate. In the air flow stream, two thermocouples were installed, the first at the inlet and the second at the outlet of the heat transfer fluid. Four other thermocouples are placed on the absorber and four thermocouples are placed on the bottom plate at identical positions along the direction of flow, for both plates. These thermocouples will permit us to follow the evolution of the temperature of the heat transfer fluid flowing through the collector at the inlet, inside the collector and finally at the outlet. The ambient temperature is also measured. The temperatures on the glass are taken using an infrared thermometer. The collector was oriented at the south direction. All experiments began at 9 am and ended at 4 pm. The measured variables are: global solar radiation, inlet and outlet temperatures of the circulating fluid through the collector, absorber plate temperatures at several selected locations, and ambient temperature.

Figures 1 and 2 show the experimental device for the closed and open cycle of air flow. Figure 3 shows a cross section of the solar collector which illustrates the location of the fins and the air flow channel. The experimentation cases are:

Case 1: Open cycle experimentation, tilt = 0 degree
Case 2: Open cycle experimentation, tilt = 30 degrees
Case 3: Closed cycle experimentation, tilt = 0 degree
Case 4: Closed cycle experimentation, tilt = 30 degrees

Table 3 shows the experimental conditions. The experiments were carried out under climatic conditions of Laghouat, Algeria. The word partial means that there is presence of clouds in the sky and clear significates sunny day. Two angles of inclination of the collector (0 and 30 degrees) are studied. The experiments were performed from 11 February 2019 to 18 February 2019 (open cycle case) and from 08 April 2019 to 14 April 2019 (closed cycle case) with the use of a single volume flow equal to 0.0129402 m³/s.

2. 3 Instrumentation provided

Thermocouples (model: DC-M02) with the characteristics (-50 to 150 °C, ±1 °C) were placed on the top surface of the absorption plate and the bottom plate at identical positions along the flow direction of the air fluid. Two thermocouples for measuring the inlet and outlet air temperatures. Four thermocouples are used for measuring the absorber temperatures and another four for measurement of the temperatures of the bottom plate. All temperatures were measured in degrees Celsius (°C). Non-contact digital infrared thermometer (model: PCE-777) (-30 to 260 °C, ±2 %) is used to measure the temperature of the ground and transparent cover.

The global solar radiation was measured with a Solarimeter (model: Kimo SL200) with the characteristics (1 à 1300 W/m², ±5 %). The flow rate was measured by a digital anemometer (model: Lutron AM-206M) with the characteristics (0.4 à 35 m/s, ±2 %). The technical characteristics of measuring devices for all instrumentation used in this study are reported in table 4.

The level of uncertainty analysis can be calculated using the method proposed by Kline and Mcclintock [21]. The uncertainty of thermal efficiency can be expressed by:

$$\omega\rho = [((Cp.\Delta T.\omega_m)/(It.Ac))^2 + ((Cp.m.\omega\Delta T)/(It.Ac))^2 + (-(Cp.m.\Delta T.\omega_m)/(It^2.Ac))^2 + ((Cp.m.\Delta T.\omega_A)/(It.Ac^2))^2]^{(1/2)} \quad (11)$$

Table 4. Technical characteristics of measuring devices.

Instrument	Measuring range	Accuracy	Resolution
Solarimeter	1 to 1300 W/m^2	5%	1 W/m^2
anemometer	0.4 to 35 m/s	± 2 %	0.1 m/s
Thermocouples	-50 to 150 °C	±1 °C	0.1 °C
Non-contact digital infrared thermometer	-30 to 260 °C	±2%	0.1 °C

Table 5. The relative uncertainty of ambient temperature (open cycle)

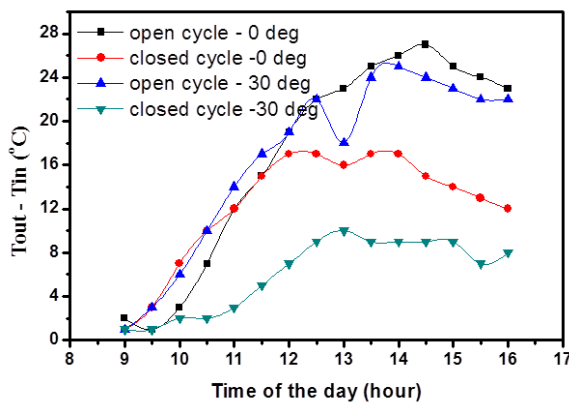| value	Open cycle (0 degree)	Relative uncertainty (%) ($\Delta T/T$)	Open cycle (30 degrees)	ΔT (°C)	Relative uncertainty (%) ($\Delta T/T$)
Minimum	11.6 °C	8.62	4.2 °C	± 1 °C	23.8
Maximum	22.8 °C	4.38	16.4 °C	± 1 °C	6.09

Figure 4. A comparison between the temperature differences ($T_{outlet} - T_{inlet}$) for all cases studied.

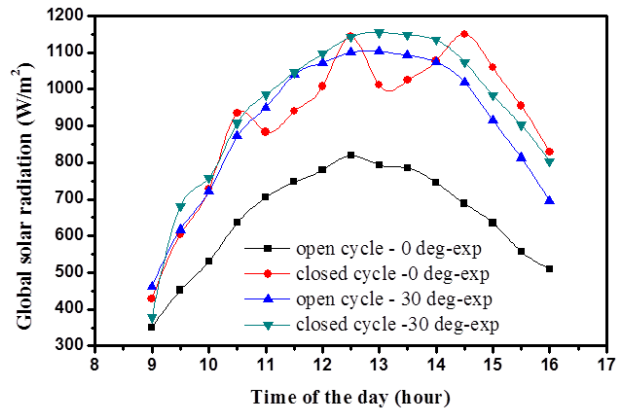**Figure 5.** The evolution of the global solar radiation (experimental) for all cases as a function of the time of the day.

With $\omega_m = \pm 2.58\text{e-}4$ kg/s, we obtained the value of uncertainty of thermal efficiency equal to ±2.19%. The relative uncertainty for the measure of temperature is calculated as follows:

Relative uncertainty (%) =
absolut eerror × 100 / measure dvalue   (12)

The absolute error is the difference between the maximum and minimum values divided by two. The relative uncertainty of ambient temperature (open cycle) results are reported in table 5.

3. Results and discussion

An experimental study was conducted to see the effect of air flow in a closed cycle (direct connection between the inlet and the air outlet) on the performance of the air collector. We establish a comparison between the results obtained for the four cases (closed cycle and open cycle). The flow rate is equal to 0.0129402 m^3/s for all cases studied. All variables are measured at a time interval of 30 minutes such as: global solar radiation, inlet and outlet air temperatures of the fluid circulating through the solar collector, ambient temperatures, and temperatures of the absorber and bottom plate.

3. 1 Temperature difference and global solar radiation

Figure 4 shows the evolution of the temperature difference ($T_{outlet} - T_{inlet}$) as a function of the time of the day for all cases studied. The highest daily solar radiation obtained is 1155 W/m^2 (closed cycle, 30 degrees) at 13h00, with the temperature difference equal

to 10 °C. After this time, the solar radiation decreased gradually and it reaches a minimum value 803 W/m^2 (16h00) as shown in figure 5. The temperature difference ($T_{outlet} - T_{inlet}$) for the open cycle (30 degrees) is higher (18 °C) as compared to the close cycle (10 °C) for the same time (closed cycle, 30 degree) (see Figure 4).

In the case 1 (open cycle, 0 degree), the maximum difference between outlet and inlet temperature occurred as 27 °C when the solar radiation reaches 688 W/m^2 for the time of the day 14h30. The solar radiation gradually decreases to minimum value of 510 W/m^2 as shown in figure 5.

For the case 2 (open cycle, 30 degree), we have obtained a global solar radiation of 1077 W/m^2, during which the temperature difference ($T_{outlet} - T_{inlet}$) reached 17 °C at 14h00. The solar radiation gradually decreases after reaching a minimum value of 695 W/m^2 (16h00) as shown in figure 5. For the open cycle configuration (0 degree), the temperature difference is higher (27 °C) as compared to the close cycle with tilt angle 0 (17 °C) (figure 4). Moreover, the temperature differences for the open cycle (0 and 30 degrees) are higher (18 – 23 °C), as compared to the close cycle (10 – 16 °C) at 13h00. The solar radiation increases with time until time but after that, it gradually decreases. It reaches a value maximum at 13h00 with intervals of (793 - 1103 W/m^2) for the open cycle (0 and 30 degrees) and (1011 - 1155 W/m^2) for the closed cycle (0 and 30 degrees) as shown in figure 5. The fluctuation of global solar radiation observed in the closed cycle (0 degree) originates from some clouds in sky.
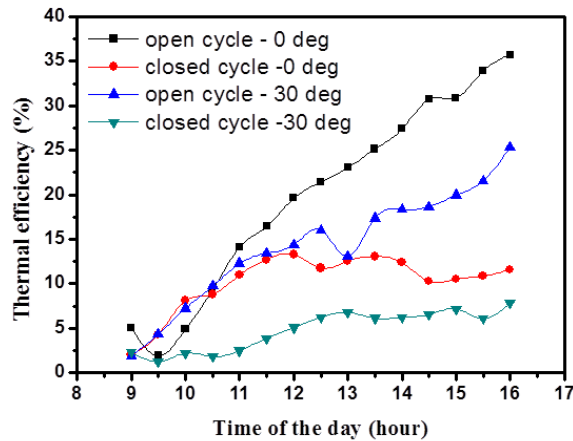
Figure 6. Variation of the thermal efficiency as function of the time of the day for all cases studied.

Table 6. The relative uncertainty of thermal efficiency (%) for open and closed cycle studied.

Time	Relative uncertainty of thermal efficiency (%)			
	Open cycle (0 degree)	Open cycle (30 degree)	Closed cycle (0 degree)	Closed cycle (30 degree)
9	43.30	111.62	107.67	94.19
9.5	112.94	50.54	51.25	171.36
10	44.90	30.24	27.04	97.72
10.5	23.54	22.45	24.82	119.22
11	15.52	17.81	19.86	87.56
11.5	13.32	16.29	17.23	56.65
12	11.15	15.23	16.45	42.96
12.5	10.20	13.66	18.60	35.23
13	9.51	16.74	17.42	32.23
13.5	8.71	12.58	16.76	35.70
14	8.00	11.92	17.68	35.27
14.5	7.13	11.74	21.33	33.40
15	7.09	10.97	20.80	30.57
15.5	6.46	10.16	20.11	35.85
16	6.13	8.66	18.85	27.84
Average value	21.86	24.04	27.73	62.38

The decrease in the temperature difference ($T_{outlet} - T_{inlet}$) and the decrease in global solar radiation at 16h00 leads in increasing in thermal efficiency as reported in figures 4 and 5. There is a slightly difference between the outlet and inlet air temperature and the decrease in the global solar radiation has led to an increase in thermal efficiency as reported in equation 6.

3. 2 Thermal efficiency
A comparison is established between the thermal efficiencies for all studied configurations as shown in figure 6. The maximum efficiencies obtained for the open cycle of both configurations were: η(30 degrees) =25.29 % and η(0 degree)=35.71% at 16h00. These values are higher than the maximum efficiencies of the closed cycle with η(30 degrees)=7.86% at 16h00 and η(0 degree)=13.31% at 12h00, respectively. The thermal efficiencies for the open cycle are higher than those of the closed cycle. It is likley due to the use of the low volume flow which has led to the appearance of the natural convection phenomenon. This, in turn, decreases

the difference between the inlet and outlet temperature and thus leads to the thermal losses due to the length of the piping (loss by convection) that joins the air inlet and outlet. The decrease in the temperature difference ($T_{outlet} - T_{inlet}$) and the decrease in the global solar radiation at 16h00 leads to an increase in the thermal efficiency as reported in figures 4 and 5. We cannot continue the experimentation after the sunshine because the global solar radiation tends to zero and thus no convection occures.

The relative uncertainty of thermal efficiency (%) for the open and closed cycles studied here for the both 0 and 30 degrees angle is reported in table 6. The average value is lower for the open cycle at 0 degree and higher for the closed cycle at 30 degrees.

3. 3 Absorber temperatures
The results presented in figure 7 show that the temperature of the absorber starts from 16.25 to 23.75 °C at the beginning of the test (09h00) and continue increasing until it reach its limit around 13h00 by a value
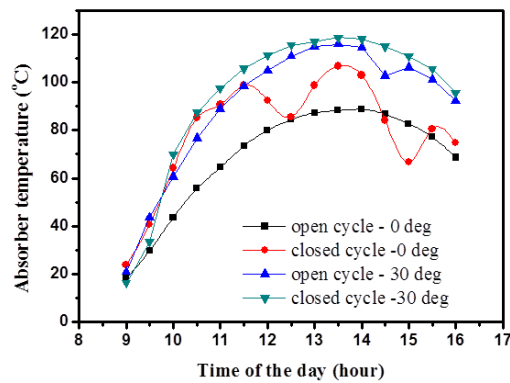
Figure 7. Evolution of the absorber temperature as function of the time of the day for the four cases.
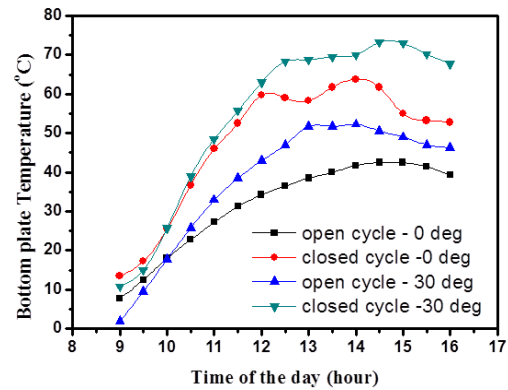

Figure 8. Evolution of the bottom plate temperature for the four cases as function of the time of the day.
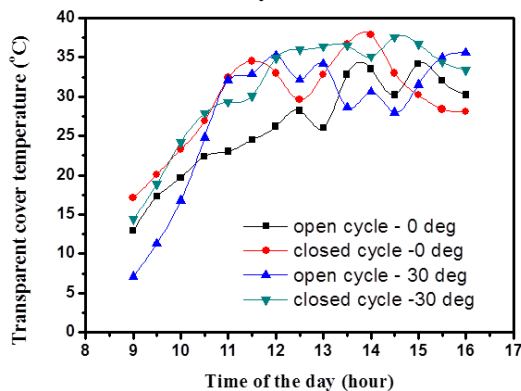

Figure 9. Evolution of the transparent cover temperature for the four cases as function of the time of the day.
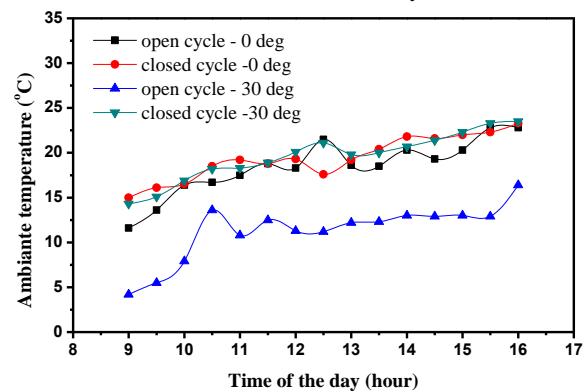

Figure 10. Evolution of the experimental ambient temperature for the four cases as function of the time of the day.

of 87.25 to 117 °C. Afterwards, it decreases to reach a value between 68.75 and 95.75 °C at 16h00, except for the closed cycle with tilt 0 degree which exhibits some fluctuations caused by the presence of clouds in sky. We observe that the temperature of the closed cycle for both inclination (0 and 30 degrees) is higher than those of the open cycle, because the inlet air temperature is equal to the ambient temperature, in the open cycle state, leading to the convection cooling for both plates (absorber and bottom plate). The fluctuation of the curve (0 degree, closed cycle) is due to the presence of clouds in the sky.

3. 4 Bottom plate temperatures
Figure 8 shows a comparison between the bottom plate temperatures as a function of the time of the day for the four studied configurations. The temperature of the bottom plate starts from 2 to 13.5 °C at the beginning of the experiment (09h00) and reaches the maximum value at 13h00. The interval of temperature is comprised between 38.5 to 68.75 °C. After that, it begins to decrease to values between 39.25 and 67.25 °C at 16h00. The bottom plate temperatures are lower than absorber temperatures for all studied cases. The interval between the blue and black curves is larger because it is a consequence of the effect of inclination angle of the solar air collector (blue curves). Increasing the useful energy, as shown in equation 9, leads to an increase in

the thermal efficiency in the open collector. It is shown that increasing the mass flow rate causes 1.5 to 4 fold increase in the collector efficiency as well as significant change in the air outlet temperature with the geometry of the absorber. This conclusion is the result of the study of Hüseyin Benli [22]. By changing the type of fins, the air flow travels larger distance before reaching to the outlet and accordingly may lead remarkable results in thermal efficiency.

3. 5 Transparent cover temperatures
Figure 9 shows the evolution of the transparent cover temperature when the time is increasing for the four configurations. The results show that the temperature of the transparent cover is slightly higher for the closed cycle for the both tilt (0 and 30 degrees), as compared with those of the open cycle. The number of points may be insufficient to obtain an average of the transparent cover temperature. The interval of temperature is comprised between 7 to 17 °C at 09h00 and 22.5 to 33 °C at 11h00. After that, it reaches an interval between 22.5 to 37 °C.

3. 6 Ambient temperatures
Figure 10 presents the variation of the experimental ambient temperature according to the variation of the time of the day for the four configurations. The ambient
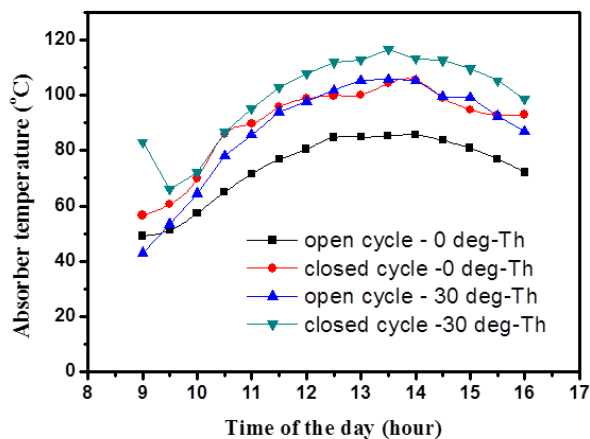
Figure 11. Evolution of the absorber temperature (theoretical) for the four studied cases as a function of the time of the day.
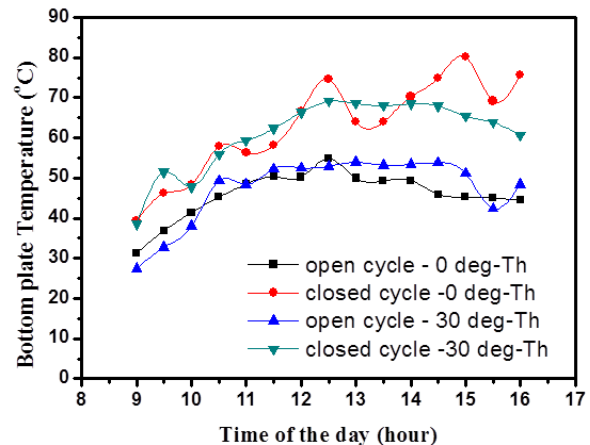

Figure 12. Evolution of the bottom plate temperature (theoretical) for the four studied cases as a function of the time of the day.

temperature effect is immediately visible on the performance of the solar collector. For the open cycle configurations, the interval of the ambient temperature corresponding to the tilt angle 0 and 30 degrees, were comprised between 11.6 to 22.8 °C and 4.2 to 16.4 °C. For the closed cycle configurations, the interval of the ambient temperature corresponding to the tilt angle 0 and 30 degrees were comprised between 15 to 23.3 °C and 14.3 to 23.5 °C, respectively. The ambient temperature was measured at a distance of 60 cm below the collector and at a distance of 1.3 m from the ground. The representation of ambient temperature curves for the various studied cases was aimed to see their changes during the day from 9h00 to 16h00 from one side and to inform the reader that the experiment was conducted in a close interval temperature, from the other side. There was no significant difference in wind speed (2 – 3 km/h) over the four days of the experiment. The solar collector starts with a very low ambient temperature, which directly influences the equations 1 to 5 and subsequently gives the numerical results presented in figures 11 and 12.

3. 7 Absorber and bottom plate temperatures (theoretical)
The mathematical formulation of the problem is taken from literature, as shown in equations 1 to 5. We used the Matlab software to develop a program that takes into account the energy balance of our solar air collector and the initial conditions of experimentation for all studied cases. Figures 11 and 12 show the evolution of the absorber and bottom plate temperatures (theoretical) for

the four cases as a function of the time of the day. The theoretical temperatures for the closed cycle are higher than the temperatures of the open cycle. This may be due to the use of the ambient temperature in the case of open cycle compared to the closed cycle where the air outlet temperature is itself the inlet. The curves of the temperature of absorber and bottom plate for the closed cycle (30 degree) are higher than the curves of the other cases studied.

4. CONCLUSIONS
In the present work, we have presented the effects of the closed air circuit cycle on the thermal performance of solar air collector with attached fins and single air pass in the region of Laghouat, Algeria. For each configuration, we have considered two tilt angle 0 and 30 degrees. A comparison between experimental and theoretical results is established. The results show that the maximum temperature difference ($T_{outlet} - T_{inlet}$) for the open cycle is higher (27 °C) (14h30) as compared to the close cycle (17 °C) (14h00). The maximum efficiencies obtained for the open cycle were η(30 degrees)=25.29% and η(0 degree)=35.71% at 16h00. These values are higher than the maximum efficiencies of the closed cycle with η(30 degree)= 7.86% at 16h00 and η(0 degree)=13.31% at 12h00. The absorber and bottom plate temperatures are higher for the closed cycle than the open cycle flow. The temperature of the transparent cover is higher in the closed cycle for the both configurations, as compared with those of the open cycle.

References
1. A R Abdulmunem, *et al., International Journal of Heat and Technology* **37,** 4 (2019) 1180.
2. D Bensahal and A Yousfi, *International Journal of Engineering* **31,** 1 (2018) 71.
3. L P Pinto, *et al.*, *International Journal of Heat and Technology* **37,** 1 (2019) 313.
4. K B Koua, EPM Koffi, and P Gbaha, *Mathematical Modelling of Engineering Problems* **5,** 4 (2018) 341.
5. F Chabane, *et al.*, *Mathematical Modelling of Engineering Problems* **6,** 1 (2019) 92.
6. A Labed, *et al.*, *International Journal of Sustainable Energy* **31,** 6 (2012) 423.
7. F Ozgen, M Esen, and H Esen, *Renewable Energy* **34,** 11 (2009) 2391.
8. M K Mittal, RP Saini, and S K Singal, *Energy* **32,** 5 (2007) 739.

9.   P Sharma and TS Bhatti, *Energy Conversion and Management* **51,** 12 (2010) 2901.
10. M Gizem, *Phd Thesis*, University of İzmir Institute of Technology, Turkey (2012)
11. F Chabane, N Moummi, and S Benramache, *Journal of Power Technologies* **93,** 1 (2013) 52.
12. HM Yeh, CD Ho, and JZ Hou, *Energy* **27,** 8 (2002) 715.
13. M Y Othman, *et al*., *Journal of Energy Engineering* **132,** 3 (2006) 121.
14. S Saurav and V N Bartaria, *International Journal of Renewable Energy Research* **3,** 3 (2013) 498.
15. A Hachemi, *International Journal of Energy Research* **19,** 7 (1995) 567.
16. HM Yeh, CD Ho, and C Y Lin, *Energy Conversion and Management* **41,** 9 (2000) 971.
17. L Goldstein Jr and EM Sparrow, *Journal of Heat Transfer* **98,** 1 (1976) 26.
18. W Gao, *et al*., *Applied Energy* **84,** 4 (2007) 425.
19. CD Ho, CW Yeh, and S M Hsieh, *Renewable Energy* **30,** 10 (2005) 1601.
20. B S Romdhane, *Solar Energy* **81,** 1 (2007) 139.
21. S J Kline and F A Mcclintock, *Journal of Mechanical Engineering* **75** (1953) 3.
22. H Benli, *Renewable Energy* **50** (2013) 58.